

# DeLTra: Deep Light Transport for Projector-Camera Systems

Bingyao Huang and Haibin Ling

Stony Brook University, NY, USA  
 {bihuang, hling}@cs.stonybrook.edu

**Abstract.** In projector-camera systems, light transport models the propagation from projector emitted radiance to camera-captured irradiance. In this paper, we propose the first end-to-end trainable solution named Deep Light Transport (DeLTra) that estimates radiometrically uncalibrated projector-camera light transport. DeLTra is designed to have two modules: DepthToAttribute and ShadingNet. DepthToAttribute explicitly learns rays, depth and normal, and then estimates rough Phong illuminations. Afterwards, the CNN-based ShadingNet renders photorealistic camera-captured image using estimated shading attributes and rough Phong illuminations. A particular challenge addressed by DeLTra is occlusion, for which we exploit epipolar constraint and propose a novel differentiable direct light mask. Thus, it can be learned end-to-end along with the other DeLTra modules. Once trained, DeLTra can be applied simultaneously to three projector-camera tasks: image-based relighting, projector compensation and depth/normal reconstruction. In our experiments, DeLTra shows clear advantages over previous arts with promising quality and meanwhile being practically convenient.

**Keywords:** Projector-camera systems, relighting, projector compensation, depth and normal reconstruction

## 1 Introduction

Projector-camera systems have many applications such as image-based relighting [23, 24, 40, 53, 55, 61, 66], projector compensation [1, 3, 6, 8, 20, 21, 28, 29, 45, 47, 58, 59, 73, 79], projection mapping [45, 60, 70, 71] and structured light [16, 42, 52, 74]. Many projector-camera applications rely on estimating the forward light transport [35], which maps the projector output radiance to the camera-captured irradiance, such that image-based relighting, projector compensation and depth/normal estimation can be performed. An example is shown in Fig. 1, where image-based relighting and depth/normal estimation are performed using the proposed deep light transport (DeLTra).

Traditionally, forward light transport is approximated by a light transport matrix (LTM) [11, 12, 51, 52, 66, 75, 83], which implicitly encodes both direct and indirect light components [46] such as diffuse, specular highlight, inter-reflections, shadow, *etc.*, without explicitly computing the scene attributes such as BRDF



Fig. 1: Deep light transport (DeLTra) for projector-camera systems: (a) scene under plain white illumination, (b) estimated normal map, (c) estimated colored point cloud viewed from a different pose, (d) a new projector input lighting pattern, (e) predicted relit result, and (f) camera-captured ground truth, *i.e.*, (d) projected to (a).

or geometry. Although full LTM [35, 51, 75] produces accurate relighting results, especially indirect light components (as we will also discuss in § 6), in most projector-camera applications, such as projection mapping, projector compensation and structured light 3-D reconstruction, direct light components dominate the light transport, thus it may be unnecessary to estimate a full LTM. Moreover, LTM-based methods usually require both camera and projector radiometric calibration [13, 19] and LTM does not explicitly recover scene geometry.

In this paper, we show that it is possible to approximate *radiometrically uncalibrated* projector-camera light transport and *explicitly* recover scene geometry. In particular, we explicitly model projector-camera light transport as a geometry- and attributes-aware shading problem and solve it using an end-to-end trainable model named **DeLTra** (Deep Light Transport), which consists of two modules: *DepthToAttribute* and *ShadingNet*.

From a learnable depth map, the **DepthToAttribute** module explicitly calculates the shading attributes such as direct light rays, surface normal, view and reflection directions, *etc.* To address the *occlusion* challenge in shading, a novel *differentiable* direct light mask is derived by exploring the related epipolar geometry, and can be efficiently computed using differentiable image warping [32], tensor sorting and image gradient. Then, rough Phong illuminations [7, 56, 67] are estimated to constrain geometry and to provide initial estimation for *ShadingNet*.

Afterwards, the **ShadingNet** module is designed to aggregate intermediate shading attributes and rough Phong illuminations, and to render photorealistic camera-captured image. Moreover, to improve model robustness and convergence, we incorporate multiple domain knowledge of projector-camera light transport, such as direct light mask consistency, rough diffuse shading consistency and depth/normal/pixel mapping smoothness.

Finally, after a few minutes of data capturing and training, three projector-camera light transport tasks, *i.e.*, *image-based relighting*, *projector compensation* and *depth/normal estimation* can be simultaneously performed by DeLTra.

Our contributions can be summarized as follows:

- The proposed DeLTra is, to our best knowledge, the first end-to-end trainable solution for radiometrically uncalibrated projector-camera light transport.

- DeLTra simultaneously performs three tasks with one learned model: image-based relighting, projector compensation and depth/normal estimation.
- For the first time, we propose a *differentiable* direct light mask to explicitly address the occlusion issue and it is expected to facilitate future works in differentiable neural rendering [27, 37, 44].
- Multiple projector-camera light transport domain knowledge is incorporated into DeLTra to improve model convergence and performance, as shown in extensive ablation studies § 5.
- The first simultaneous image-based relighting and depth/normal estimation benchmark is constructed, which is expected to facilitate future works in this direction.

The source code, benchmark and experimental results will be publicly available upon the acceptance of the paper.

## 2 Related Works

Light transport is the propagation from incident light field to outgoing light field and can be modeled using a full 8-D light transport field [35]. For a projector-camera pair that has fixed poses and 2-D image planes, the full 8-D light transport field can be reduced to a 4-D light transport matrix (LTM) [11, 12, 52, 61, 66, 75, 83], such that each camera pixel’s irradiance is a linear combination of *all* projector pixels’ radiances. Light transport studies can be roughly categorized into three types: general forward light transport [11, 12, 40, 48, 52, 53, 55, 61, 66, 75, 83], inverse light transport [1, 3, 6, 20, 45, 47, 49, 50, 58, 59, 65, 79] and attributes from shading [10, 16, 36, 42, 52, 64, 69, 72, 74, 78].

**General light transport** Early methods [12, 77] directly estimate LTM using brute force sampling which requires plenty captures, memory and time. To improve LTM estimation efficiency, later methods exploit the sparsity and coherence of LTM [11, 40, 48, 55, 61, 66, 75, 83], leading to reduced sampling images and computation.

Inverse light transport aims to estimate the input light given a camera-captured image. It has many applications such as decomposing a camera-captured image into direct and indirect light components [4, 9, 65], synthesizing new light patterns for scene appearance editing [1, 70] and projector compensation [3, 6, 20, 45, 47, 49, 58, 59, 79].

Despite free of scene modeling, estimating full forward LTM is time consuming and impractical in some projector-camera applications. Leveraging the independence of projector pixels, some studies [20, 21, 47] simplify LTM and assume each camera pixel is only coupled with a *single* projector pixel that contributes most of the (ir)radiance, *i.e.*, direct light only. Then projector and camera pixel-wise mapping can be applied to efficiently solve *projector compensation* and *attributes from shading*.

In this paper, we focus on light transport for projector-camera system applications, such as projection mapping, projector compensation and structured light 3-D reconstruction, where direct light components dominate the light transport, hence it is different from general light transport. Extending the proposed method to general light transport is definitely an interesting direction to explore.

**Projector compensation** Projector compensation estimates a projector input image given its corresponding desired camera-captured image and can be roughly categorized into full compensation, *i.e.*, both geometric and photometric compensation and partial ones. Detailed reviews can be found in [6, 22], and some recent representative works can be found in [21] and [28, 29].

**Attributes from shading** Attributes from shading [5] aims to estimate scene attributes involved in light transport, such as surface normal, reflectance, light directions and depth, *etc.* To avoid complex indirect light modeling, some simplifications are imposed, such as assuming distant light in photometric stereo (PS) or direct light dominance in structured light (SL), respectively. In the following we briefly review studies in PS and SL that most relate to our work.

*Photometric stereo* [10, 64, 69, 72, 78] estimates surface normal by varying the light directions while fixing the view direction. In its earliest form [78] the surface is assumed Lambertian and the surface normal is obtained by solving linear equations. More complex BRDFs are considered [17, 68] later. Recently, Santo *et al.* [64] leverage deep neural networks to solve this problem using supervised training data. To avoid creating normal ground truth, Taniar *et al.* [72] propose a self-supervised photometric stereo network that uses image reconstruction loss. To deal with uncalibrated cases, Chen *et al.* [10] propose a self-calibrating method to jointly estimate unknown light directions and surface normal from non-Lambertian surfaces.

*Structured light* (SL) [16, 36, 42, 52, 74] estimates scene depth by matching projected and captured hand-crafted patterns, then matched 2-D pixel coordinates are triangulated [25] to recover the 3-D point cloud. However, this two-step strategy heavily depends on direct light and thus 2-D pixel matching may fail in strong indirect light regions [11, 28, 52]. To address this issue, O’Toole *et al.* [52] combine LTM with SL to jointly estimate scene depth, albedo and indirect light.

Although PS and SL can recover the geometry of the scene, they alone are unable to solve image-based relighting or projector compensation with complex indirect light components [46], such as occlusion, specular highlight, inter-reflections and caustics, *etc.*, as shown in Fig. 5 and Fig. 6.

**Relationship to DeLTra** Recently, deep learning-based solutions are proposed for special cases of light transport, such as deep shading/neural rendering [27, 37, 44], projector compensation [28, 29] and attributes from shading [14, 38, 39, 57, 80]. However, these methods either require scene modeling or have simple assumptions on scene geometry, or need ground truth attributes supervision.

The question is, for a radiometrically uncalibrated projector-camera system, can we estimate the light transport and apply it *simultaneously* to three tasks, *i.e.*, image-based relighting, projector compensation and depth/normal reconstruction? The study in [28] shows it is possible for projector compensation, but it makes simple assumptions on scene geometry and hence restricted to smooth occlusion-free surfaces. Moreover, the 3-D geometry and shading attributes involved in inverse light transport are ignored. Both limitations make it unable to perform image-based relighting in general scenes with occlusions or depth/normal reconstruction. Thus, directly applying CNNs to projector-camera light transport is hard without leveraging the domain knowledge. By

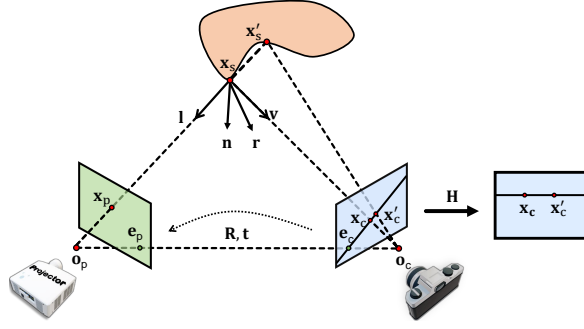


Fig. 2: Coordinate system of a projector-camera system. With the geometric calibration, a rectification transformation  $\mathbf{H}$  can be calculated to transform the camera-captured image such that all epipolar lines are parallel.

contrast, DeLTra approximates projector-camera light transport and performs image-based relighting, projector compensation and depth/normal estimation with a fully trainable deep model, meanwhile waiving projector-camera radiometric calibration.

### 3 Deep Light Transport for Projector-Camera Systems

#### 3.1 Problem formulation

**Projector-camera setup.** As shown in Fig. 2, we assume the world origin is at camera optical center  $\mathbf{o}_c$  and denote camera and projector intrinsics as  $\mathbf{K}_c$  and  $\mathbf{K}_p$ , denote their relative rotation and translation as  $\mathbf{R}$  and  $\mathbf{t}$ . Let  $\mathbf{x}_c, \mathbf{x}_p \in \mathbb{R}^2$  be pixel coordinates of a surface point  $\mathbf{x}_s \in \mathbb{R}^3$  in camera image  $\mathbf{I}_c$  and projector image  $\mathbf{I}_p$ , respectively. Denote the depth of  $\mathbf{x}_s$  as  $d_c = \mathbf{d}_c(\mathbf{x}_c)$ , where  $\mathbf{d}_c \in \mathbb{R}^{h \times w \times 1}$  is the depth map in camera’s view (Fig. 3). The geometric relationships between  $\mathbf{x}_s$ ,  $\mathbf{x}_c$  and  $\mathbf{x}_p$  are given by:

$$\mathbf{x}_s = \mathbf{K}_c^{-1} \bar{\mathbf{x}}_c d_c; \quad \bar{\mathbf{x}}_p = \mathbf{K}_p[\mathbf{R}|\mathbf{t}]\bar{\mathbf{x}}_s \quad (1)$$

where  $\bar{\mathbf{x}}$  stands for homogeneous coordinate of  $\mathbf{x}$ . Given the projector and camera pixel mappings in Eq. 1, projector direct light pixel values aligned with camera’s view are given by:

$$\mathbf{I}'_p = \phi(\mathbf{I}_p, \mathbf{\Omega}), \quad \mathbf{x}_p = \mathbf{\Omega}(\mathbf{x}_c) \quad (2)$$

where  $\mathbf{\Omega} \in \mathbb{R}^{h \times w \times 2}$  is the image sampling grid and  $\phi$  the image interpolator.

In addition, projector ray direction  $\mathbf{l}$ , reflection ray direction  $\mathbf{r}$  and camera view direction  $\mathbf{v}$  are given by:

$$\mathbf{n} = \nabla_x \mathbf{x}_s \times \nabla_y \mathbf{x}_s; \quad \mathbf{l} = \mathbf{o}_p - \mathbf{x}_s; \quad \mathbf{v} = \mathbf{o}_c - \mathbf{x}_s; \quad \mathbf{r} = 2(\mathbf{n} \cdot \mathbf{l})\mathbf{n} - \mathbf{l} \quad (3)$$

where operator  $\times$  is vector cross product.

**Projector-camera light transport.** In the above system, the camera-captured irradiance at surface point  $\mathbf{x}_s$  can be formulated by the rendering equation<sup>1</sup> [33]:

$$L_c(\mathbf{v}) = L_d(\mathbf{l}, \mathbf{v}) + \int_W f_s(\omega_i, \mathbf{v}) L_i(\omega_i)(\omega_i \cdot \mathbf{n}) d\omega_i \quad (4)$$

<sup>1</sup> For conciseness, we omit  $\mathbf{x}_s$  in the equation.

where  $L_c(\mathbf{v})$ ,  $L_d(\mathbf{l}, \mathbf{v})$  and  $L_i(\omega_i)$  are camera-captured irradiance, surface direct light (first-bounce) radiance corresponding to the projector and surface incident indirect light (n-bounce) radiances, respectively.  $f_s$  and  $\omega_i$  are surface BRDF and surface incident *indirect* light direction, respectively.

A typical solution to Eq. 4 is to discretize it and model projector and camera (ir)radiance mappings as linear operations [2, 50, 65]:

$$\mathbf{L}_c = \mathbf{L}_d + \mathbf{L}_i = \mathbf{T}\mathbf{L}_p \quad (5)$$

where  $\mathbf{T}$  is the light transport matrix [2, 12, 50, 52, 65, 66, 83] that implicitly encodes direct light  $\mathbf{L}_d$ , indirect light  $\mathbf{L}_i$  and geometry.  $\mathbf{L}_c$  and  $\mathbf{L}_p$  are camera-captured and projector output RAW (ir)radiances, respectively. If camera's and projector's nonlinear radiometric response functions [13, 19]  $f_c$  and  $f_p$  are known, we can obtain both  $\mathbf{L}_c = f_c^{-1}(\mathbf{I}_c)$  and  $\mathbf{L}_p = f_p(\mathbf{I}_p)$ , where  $\mathbf{I}_c$  and  $\mathbf{I}_p$  are camera-captured and projector input RGB images. Then,  $\mathbf{T}$  can be solved using image pairs like  $\mathbf{L}_c$  and  $\mathbf{L}_p$ . In this paper, we are interested in a special light transport case for radiometrically uncalibrated projector-camera systems (*i.e.*, unknown  $f_c$  and  $f_p$ ) under the direct light dominance assumption. Moreover, we aim to *explicitly* recover the geometry from the discretized light transport in Eq. 5. We start by extending Eq. 5 to incorporate nonlinear radiometric response functions  $f_c$  and  $f_p$  and shading attributes  $f_s(\cdot)$ ,  $\mathbf{n}$ ,  $\mathbf{l}$  and  $\mathbf{v}$ <sup>2</sup>:

$$\mathbf{I}_c = f_c(\mathbf{T}f_p(\mathbf{I}_p)) = \pi(\mathbf{I}_p, f_s(\cdot), \mathbf{n}, \mathbf{l}, \mathbf{v}) \quad (6)$$

where  $\pi$  is the radiometrically uncalibrated light transport from projector input RGB image  $\mathbf{I}_p$  to camera-captured RGB image  $\mathbf{I}_c$ . Apparently Eq. 6 has no closed form solution and one intuition is to directly approximate  $\pi$  from sampling image pairs like  $\mathbf{I}_c$  and  $\mathbf{I}_p$  using an image-to-image translation CNN, *e.g.*, U-Net [63]. However, as described in [28], direct learning complex transformations like Eq. 6 using CNN is hard without incorporating light transport domain knowledge.

As for projector-camera light transport, we have multiple shading domain knowledge. Observing Eq. 6 and relax it using *direct light dominance* assumption, we can encode surface BRDF  $f_s(\cdot)$ , geometry such as projector ray direction  $\mathbf{l}$ , camera view direction  $\mathbf{v}$  and surface normal  $\mathbf{n}$  in rough Phong illumination [7, 56, 67]. Then, we reformulate Eq. 6 as a transformation from rough Phong illumination to refined photorealistic shadings in the below equation:

$$\mathbf{I}_c = \mathcal{F}(\mathbf{I}'_p, \mathbf{I}_c^{\text{abnt}}, \mathbf{I}_c^{\text{diff}}, \mathbf{I}_c^{\text{spec}}) \quad (7)$$

where  $\mathcal{F}$  is a nonlinear image-to-image transformation,  $\mathbf{I}'_p$  is the projector direct light pixel values in camera view (Eq. 2).  $\mathbf{I}_c^{\text{abnt}}$ ,  $\mathbf{I}_c^{\text{diff}}$  and  $\mathbf{I}_c^{\text{spec}}$  are rough ambient, diffuse and specular components and are given by:

$$\mathbf{I}_c^{\text{abnt}} = \mathbf{s}, \quad \mathbf{I}_c^{\text{diff}} = \mathbf{I}'_p \odot \mathbf{s} \odot (\mathbf{n} \cdot \mathbf{l}), \quad \mathbf{I}_c^{\text{spec}} = \mathbf{I}'_p \odot \dot{\mathbf{s}} \odot (\mathbf{r} \cdot \mathbf{v})^\alpha \quad (8)$$

where  $\mathbf{s}$  (Fig. 3) models rough ambient component and surface reflectance and is approximated by a scene image captured under plain white illumination;  $\odot$

<sup>2</sup> We abuse the notation and refer  $\mathbf{n}$ ,  $\mathbf{l}$ ,  $\mathbf{v}$  and  $\mathbf{r}$  as  $\mathbb{R}^{h \times w \times 3}$  maps in the following text.

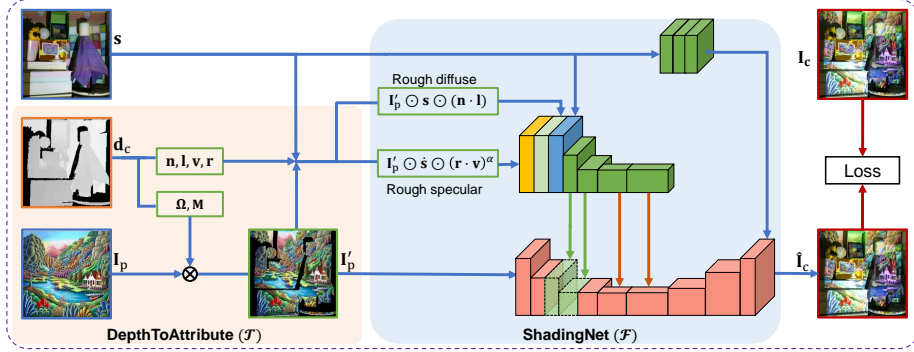


Fig. 3: DeLTra architecture. The learnable depth map  $\mathbf{d}_c$  and ShadingNet  $\mathcal{F}$  are jointly optimized during training. Firstly, using DepthToAttribute  $\mathcal{T}$ , we compute the shading attributes, *i.e.*,  $\mathbf{n}, \mathbf{l}, \mathbf{r}, \mathbf{v}, \mathbf{M}$  and projector direct light intensity  $\mathbf{I}'_p = \phi(\mathbf{I}_p, \mathbf{\Omega})$ ,  $\otimes$  is a bilinear interpolator  $\phi$ . Then, we compute rough Phong diffuse and specular components. Finally, the ShadingNet  $\mathcal{F}$  takes four inputs: (1) rough ambient, *i.e.*, the camera-captured surface image  $\mathbf{I}_c^{\text{abnt}} = \mathbf{s}$ , (2) rough diffuse  $\mathbf{I}_c^{\text{diff}}$ , (3) rough specular  $\mathbf{I}_c^{\text{spec}}$ , and (4) projector direct light intensity  $\mathbf{I}'_p$ , to render photorealistic camera-capture image  $\hat{\mathbf{I}}_c$ .

and  $\cdot$  are element-wise multiplication and dot product, respectively;  $\dot{\mathbf{s}}$  is the grayscale image of  $\mathbf{s}$ . Note that rather than using the actual diffuse, specular reflectance maps and shininess, we use a camera-captured surface image instead and set shininess  $\alpha = 1$ . The reasons are (1) estimating actual diffuse and specular reflectance maps are difficult; and (2) even with accurate diffuse and specular reflectance maps, the empirical model alone cannot produce photorealistic rendering. Therefore, the rough shadings only provide a simple yet reasonable initial point, meanwhile leveraging shading attributes domain knowledge.

Then, we design  $\mathcal{F}$  (Eq. 7) as a deep CNN named **ShadingNet** to aggregate rough shadings and to infer photorealistic direct/indirect light components as shown in Fig. 3. Note that we pass rough ambient component  $\mathbf{I}_c^{\text{abnt}} = \mathbf{s}$  to the output layer, allowing  $\mathcal{F}$  to focus on learning direct/indirect light residuals [26] on top of  $\mathbf{s}$  instead of directly predicting the final shading from scratch.

To obtain the necessary shading attributes in Eq. 7, such as projector ray direction  $\mathbf{l}$ , camera view direction  $\mathbf{v}$  and surface normal  $\mathbf{n}$ , we aggregate Eq. 1-Eq. 3 and design a differentiable module **DepthToAttribute**  $\mathcal{T}$  to explicitly compute shading attributes from the learnable depth map  $\mathbf{d}_c$  and projector-camera intrinsics and extrinsics:

$$\{\mathbf{n}, \mathbf{l}, \mathbf{r}, \mathbf{v}, \mathbf{\Omega}\} = \mathcal{T}(\mathbf{d}_c, \mathbf{K}_c, \mathbf{K}_p, \mathbf{R}, \mathbf{t}) \quad (9)$$

With projector-camera geometric calibration [30], a surface image  $\mathbf{s}$  and sampling image pairs like  $(\mathbf{I}_c, \mathbf{I}_p)$ , we can learn to approximate the radiometrically uncalibrated light transport function  $\pi_\theta = \{\mathcal{T}, \mathcal{F}\}_\theta$  using a deep CNN and a learnable depth map  $\mathbf{d}_c$ .



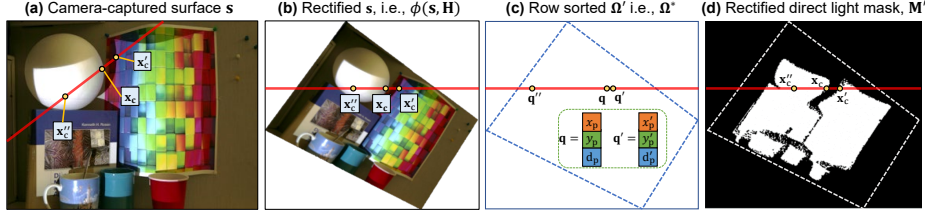


Fig. 4: Proposed differentiable direct light mask. (a) Three points are on the same red epipolar line and finding occlusion requires 2-D searching. (b) Instead, we perform 1-D search in stereo rectified image. (c) To speed up pair-wise comparison, we row sort  $\Omega'$  in lexicographic order. After sorting,  $\mathbf{x}_c$ 's and  $\mathbf{x}'_c$ 's corresponding points  $\mathbf{q}, \mathbf{q}' \in \Omega^*$  become neighbors, then we apply Eq. 11 and find that  $\mathbf{x}'_c$  is occluded, since  $|x'_p - x_p| + |y'_p - y_p| < 1$  and  $|d'_p - d_p| > 0$ . All operations are differentiable and parallelizable, thus are efficient for training on GPU.

### 3.2 Differentiable direct light mask

The depth-based image warping in Eq. 2 is unable to solve occlusion ambiguity, *i.e.*, as shown in Fig. 2 and Fig. 4 multiple camera pixels can map to the same projector pixel, causing false projector direct light rays. To address this issue, some stereo vision and optical flow methods [15, 18, 31, 41, 76] leverage forward-backward consistency to find occlusions, under the assumption that slight motion and lighting changes across views. However, for a projector-camera system the projector input and camera-captured images have significant photometric and geometric inconsistency. Therefore, we exploit epipolar geometry instead and propose a *differentiable* direct light mask to address occlusions below.

As shown in Fig. 2 and Fig. 4, surface points  $\mathbf{x}_s$  and  $\mathbf{x}'_s$  lie on the same projector ray. Their camera image projections are  $\mathbf{x}_c$  and  $\mathbf{x}'_c$ , respectively. According to epipolar geometry,  $\mathbf{x}_c$  and  $\mathbf{x}'_c$  must lie on the same epipolar line. From Fig. 2 and Fig. 4, we see that  $\mathbf{x}'_s$  is occluded by  $\mathbf{x}_s$  and only  $\mathbf{x}_c$  is illuminated by projector direct light. From this observation, we create a direct light mask  $\mathbf{M}$  to indicate direct light pixels and occluded pixels. For any camera pixel  $\mathbf{x}_c$  on epipolar line  $\overrightarrow{\mathbf{e}_c \mathbf{x}'_c}$  ( $\mathbf{e}_c$  is the camera epipole), its pixel value in  $\mathbf{M}$  is given by:

$$\mathbf{M}(\mathbf{x}_c) = \begin{cases} 1, & \forall \mathbf{x}'_c \in \overrightarrow{\mathbf{e}_c \mathbf{x}'_c}, \mathbf{x}_p \not\approx \mathbf{x}'_p \vee d_p < d'_p \\ 0, & \text{otherwise} \end{cases} \quad (10)$$

where  $\mathbf{x}_p = \Omega(\mathbf{x}_c)$  and  $\mathbf{x}'_p = \Omega(\mathbf{x}'_c)$  are the corresponding projector pixel coordinates, respectively (Fig. 2).  $d_p = ([\mathbf{R}|\mathbf{t}]\bar{\mathbf{x}}_s)_z$  and  $d'_p = ([\mathbf{R}|\mathbf{t}]\bar{\mathbf{x}}'_s)_z$  are the depths ( $z$  coordinates) of  $\mathbf{x}_c$  and  $\mathbf{x}'_c$  in projector view space. To speed up computation, we apply stereo rectification [25]  $\mathbf{H}$  to reduce the 2-D search to 1-D (Fig. 4(b)).

Even with 1-D search, however, the pair-wise comparison in Eq. 10 for each pixel on each epipolar line is computationally expensive. The logical or condition in Eq. 10 implies that depth comparison is only needed when  $\mathbf{x}_c$  and  $\mathbf{x}'_c$  map to the same *projector* pixel, *i.e.*,  $\mathbf{x}_p \approx \mathbf{x}'_p$  (Fig. 2). For example in Fig. 4(a), although  $\mathbf{x}'_c$  is also on the epipolar line, it does not occlude  $\mathbf{x}_c$  because  $\mathbf{x}''_p \not\approx \mathbf{x}'_p$ .



Therefore, for each *rectified* epipolar line, if we sort each pixel’s corresponding projector pixel coordinates  $\mathbf{x}_p$  in lexicographical order, the pair-wise comparisons in Eq. 10 can be performed only in a small neighborhood, *e.g.*,  $\pm 1$  pixel.

To make the above operations *differentiable*, we concatenate the sampling grid  $\Omega$  and the projector-view depth map  $\mathbf{d}_p$  along the third dimension and rectify them using differentiable bilinear interpolator [32] as  $\Omega' = \phi([\Omega, \mathbf{d}_p], \mathbf{H})$ ,  $\Omega' \in \mathbb{R}^{h \times w \times 3}$ . Next, we sort each  $3 \times 1$  element in each row of  $\Omega'$  (*i.e.*, along epipolar line) in lexicographical order and denote the sorted tensor  $\Omega'$  as  $\Omega^*$  (Fig. 4(c)). Afterwards, we compute the forward difference in row direction, then a pixel in rectified direct light mask  $\mathbf{M}'$  is given by:

$$\mathbf{M}' = \begin{cases} 1, & |\nabla \Omega_x^*| + |\nabla \Omega_y^*| > 1 \vee \nabla \Omega_z^* < 0 \\ 0, & \text{otherwise} \end{cases} \quad (11)$$

Note the non-differentiable unit step function above is approximated by differentiable clamping and ReLU [43] as:  $\min(\sigma * \text{ReLU}(\cdot), 1)$ ,  $\sigma \gg 1$ . Then, we unrectify mask  $\mathbf{M}'$  (Fig. 4(d)) back to camera’s view by  $\mathbf{M} = \phi(\mathbf{M}', \mathbf{H}^{-1})$ . Finally, direct light mask is applied to mask out false direct light pixels in warped projector image  $\mathbf{I}'_p \leftarrow \mathbf{I}'_p \odot \mathbf{M}$ , and to enforce direct light mask consistency below.

### 3.3 Additional domain knowledge

Besides rough shadings and direct light mask, we introduce three additional constraints to ensure accurate shading attributes prediction and prevent  $\mathcal{F}$  from overfitting. Their effectiveness is shown later in ablation study.

**Direct light mask consistency** ensures that predicted direct light mask  $\mathbf{M}$  matches camera-captured projector FOV  $\mathbf{s}^*$ . It can reduce depth searching space by early rejecting geometrically impossible depths and is implemented as a penalty on pixel-wise  $l_2$  loss:

$$\mathcal{L}_{\text{mask}} = \|\mathbf{M} - \mathbf{s}^*\|^2 \quad (12)$$

where  $\mathbf{s}^*$  is a thresholded camera-captured surface image for projector FOV.

**Rough shading consistency** encourages photometric similarities between rough diffuse shading  $\mathbf{I}_c^{\text{diff}}$  and camera-captured ground truth  $\mathbf{I}_c$ :

$$\mathcal{L}_{\text{rough}} = \|\mathbf{I}_c^{\text{diff}} - \mathbf{I}_c\|^2 \quad (13)$$

This loss forces DeLTra to predict plausible light rays and surface normal map.

**Smoothness.** We also enforce the weighted smoothness [15, 18, 82] of the depth map, sampling grid and normal map. It prevents  $\mathcal{F}$  from overfitting on coarse input attributes in early training stages.

$$\mathcal{L}_{\text{smooth}} = \mathcal{L}_{\text{smooth}}(\mathbf{d}_c) + \mathcal{L}_{\text{smooth}}(\Omega) + 0.01\mathcal{L}_{\text{smooth}}(\mathbf{n}) \quad (14)$$

### 3.4 One stone three birds

Once trained, the proposed DeLTra can be used for three tasks: image-based relighting, projector compensation and depth/normal estimation.

**Relighting** predicts the camera-captured image given a novel projector input  $\mathbf{I}_p$  without actual projection. It is performed by a single forward pass of DeLTra, since DeLTra learns the forward lighting transport  $\mathbf{I}_p \mapsto \mathbf{I}_c$  (Eq. 6).

**Compensation** predicts a projector input image  $\mathbf{I}_p^*$ , named compensation image, given a desired camera-captured image  $\mathbf{I}_c$  and can be solved with a loss function  $\mathcal{L}_{\text{compen}}$  consisting of pixel-wise  $l_1$  image reconstruction loss, compensation image smoothness loss and saturation loss [21]:

$$\mathbf{I}_p^* = \arg \min_{\mathbf{I}_p} \mathcal{L}_{\text{compen}}(\mathbf{I}_p, \mathbf{I}_c), \text{ where} \quad (15)$$

$$\mathcal{L}_{\text{compen}} = |\pi(\mathbf{I}_p) - \mathbf{I}_c| + 0.1\mathcal{L}_{\text{smooth}}(\mathbf{I}_p) + \|\mathbf{I}_p[\mathbf{I}_p > 1] - 1\|^2 + \|\mathbf{I}_p[\mathbf{I}_p < 0]\|^2 \quad (16)$$

**Depth and normal** are inherently learned by DeLTra in  $\mathbf{d}_c$  and  $\mathcal{T}$ . To be robust against setup scale variances, we normalize the depth and translation vector  $\mathbf{t}$  by dividing  $\|\mathbf{t}\|$ , the actual scene depth is given by denormalization:  $\hat{\mathbf{d}}_c = \mathbf{d}_c * \|\mathbf{t}\|$ .

## 4 Network Architecture

The proposed DeLTra consists of two subnets: a depth-based attribute computation module **DepthToAttribute** ( $\mathcal{T}$ ) and a **ShadingNet** ( $\mathcal{F}$ ) that synthesizes camera-captured image using the attributes from  $\mathcal{T}$  as shown in Fig. 3. This architecture is inspired by [28] that disentangles projector-camera inverse light transport  $\pi^\dagger$  as a 2-D image warping module  $\mathcal{T}$  and a photometric compensation module  $\mathcal{F}$ . Here we follow [28]’s convention and use the same symbols  $\mathcal{F}$  and  $\mathcal{T}$ .

**DepthToAttribute** ( $\mathcal{T}$ ) contains a learnable depth map  $\mathbf{d}_c$  and computes the shading attributes (Eq. 9) and a direct light mask  $\mathbf{M}$  (§ 3.2). Then, the shading attributes are used for rough Phong illuminations computation (Eq. 8).

**ShadingNet** ( $\mathcal{F}$ ) extends CompenNet++ [28]’s  $\mathcal{F}$  by the following improvements, (1) CompenNet++ aims to predict the projector input image (*i.e.*, inverse light transport), while ShadingNet aims to predict the camera-captured image (*i.e.*, forward light transport). (2) ShadingNet explicitly computes rough Phong illuminations and refine direct/indirect light on top of it. (3) The surface branch features are both added and concatenated (green blocks) to the backbone branch, allowing learning more complex light and attributes interactions.

The novel DepthToAttribute module, *differentiable* direct light mask, improved ShadingNet and domain knowledge together let DeLTra efficiently model radiometrically uncalibrated projector-camera light transport and outperform compared counterparts by a significant margin as shown in § 5.

**Loss function.** Combining the image reconstruction loss and the losses in § 3.3, our final loss function is

$$\mathcal{L} = \mathcal{L}_{\text{recon}} + \mathcal{L}_{\text{mask}} + \mathcal{L}_{\text{smooth}} + \mathcal{L}_{\text{rough}} \quad (17)$$

where  $\mathcal{L}_{\text{recon}}$  is the pixel-wise  $l_1$ +SSIM loss between the predicted camera-captured image  $\hat{\mathbf{I}}_c = \pi(\mathbf{I}_p)$  and the ground truth  $\mathbf{I}_c$ . The advantages of this image reconstruction loss are shown in [28, 29, 81].

Table 1: Quantitative comparison of relighting and depth reconstruction on different #Train. Results are averaged over 23 different setups.  $\mathbf{d}_{\text{err}}$  is the mean  $l_2$  distance between the predicted and the ground truth point cloud (mm). For SL [42] without manual cleaning and interpolation,  $\mathbf{d}_{\text{err}} = 1.0858$ .

# Train	Model	SL Masked			Whole Image			
		PSNR $\uparrow$	RMSE $\downarrow$	SSIM $\uparrow$	PSNR $\uparrow$	RMSE $\downarrow$	SSIM $\uparrow$	$\mathbf{d}_{\text{err}} \downarrow$
50	TPS + SL	27.6703	0.0731	0.9407	17.8285	0.2345	0.4336	-
	DeLTra	27.7654	0.0734	0.9403	26.0128	0.0899	0.8911	9.1092
	No rough	26.7590	0.0819	0.9292	25.2819	0.0971	0.8794	12.1576
	No mask	27.1808	0.0786	0.9320	25.5499	0.0947	0.8800	13.1909
	No const.	26.8483	0.0810	0.9298	25.3127	0.0967	0.8781	10.9433
	CompenNet++	24.2998	0.1093	0.8991	23.3141	0.1220	0.8437	-
100	TPS + SL	27.6165	0.0736	0.9439	17.8261	0.2346	0.4365	-
	DeLTra	29.3317	0.0608	0.9555	27.1247	0.0788	0.9082	5.4826
	No rough	28.4436	0.0674	0.9480	26.5000	0.0845	0.8984	6.4155
	No mask	29.2334	0.0614	0.9538	27.0299	0.0794	0.9048	6.7181
	No const.	28.4672	0.0672	0.9478	26.5230	0.0843	0.8982	6.4321
	CompenNet++	26.7337	0.0817	0.9329	25.3195	0.0961	0.8849	-
250	TPS + SL	27.4265	0.0753	0.9444	17.8056	0.2352	0.4369	-
	DeLTra	30.3590	0.0534	0.9644	27.9482	0.0713	0.9210	3.2100
	No rough	29.7556	0.0575	0.9585	27.5128	0.0750	0.9122	3.5236
	No mask	30.5538	0.0522	0.9647	28.0467	0.0704	0.9197	3.5173
	No const.	29.8096	0.0571	0.9588	27.5576	0.0745	0.9127	3.4347
	CompenNet++	26.7593	0.0810	0.9322	25.3926	0.0947	0.8860	-
500	TPS + SL	27.2926	0.0766	0.9436	17.7908	0.2356	0.4362	-
	DeLTra	30.7768	0.0509	0.9673	28.2999	0.0685	0.9247	2.4149
	No rough	30.2558	0.0540	0.9619	27.9209	0.0715	0.9166	2.5538
	No mask	30.9930	0.0495	0.9675	28.4164	0.0675	0.9233	2.5263
	No const.	30.2597	0.0540	0.9621	27.9260	0.0714	0.9168	2.6149
	CompenNet++	27.4843	0.0743	0.9386	26.0587	0.0879	0.8948	-

**System configuration and implementation.** The proposed DeLTra setup consists of a radiometrically uncalibrated Canon 6D camera and a ViewSonic PJD7828HDL DLP projector and they are geometrically calibrated using the method in [30]. Their resolutions are  $320 \times 240$  and  $800 \times 600$ , respectively.

We implement DeLTra using PyTorch [54] and Kornia [62] and optimize it using Adam optimizer [34]. The initial learning rate of depth map  $\mathbf{d}_c$  and ShadingNet  $\mathcal{F}$  are set to  $10^{-2}$  and  $10^{-3}$ , respectively. In addition, the penalty factor of ShadingNet is set to  $10^{-4}$ . Then, we train the model for 1,000 iterations and different number of training images (#Train in Tab. 1) on three Nvidia GeForce 1080Ti GPUs with a batch size of 24, and it takes about 5min to finish.

## 5 Experimental Evaluations

**Evaluation benchmark** Following [28], we capture 23 different setups with various lightings, poses and focal lenses. Using the sampling patterns in [28], we capture #Train training images (takes 3min) for training and another 200 images for testing. We then capture projector compensation setups, unlike relighting, compensation aims to generate visually pleasing projection, thus we assume the whole projector FOV can only have slight occlusions. Furthermore, we capture more complex scenes with glasses and partial projector FOV out-of-view to show that the proposed DeLTra outperforms the other methods. However, these scenarios may cause missing pixels and thus is unfair to use the surrogate protocol in [28]. Instead, we compare on camera-captured compensations.



Fig. 5: **Image-based relighting.** For TPS+SL, since SL is unable to find pixel mappings in indirect light regions such as shadows, specular highlight and translucency, thus these areas are black. CompenNet++ generates blurred relit images, since both its 2-D warping and simple CNN cannot well solve complex geometry and indirect light involved in projector-camera forward light transport. See [supplementary material](#) for more results.

Afterwards, we capture the ground truth point cloud using SL [42], followed by human-aided cleaning and interpolation. Future works on projector-camera image-based relighting and depth/normal reconstruction can be evaluated and compared with DeLTra without actual projections.

**Relighting** To the best of our knowledge, existing image-based relighting methods rely on radiometric calibration, thus we cannot compare with them using our radiometrically uncalibrated setup. Instead, we modify the recently proposed projector compensation method CompenNet++ [28] by swapping its input and output, such that forward light transport can be estimated. We train it with the same batch size and iterations as DeLTra, and it also takes 5min.

The results in Fig. 5 and Tab. 1 show that the proposed DeLTra significantly outperforms CompenNet++, our explanations are (1) DeLTra explicitly models projector-camera light transport geometry and shading attributes such as depth, normal and light directions and imposes additional domain knowledge, *e.g.*, rough shadings, mask consistencies and smoothness, such that both improve the performance and convergence of the model. (2) CompenNet++’s 2-D warping-based geometric correction is unable to address occlusions, while DeLTra predicts a differentiable direct light mask to explicitly deal with occlusions. (3) Our ShadingNet refines rough shadings and has a novel structure that allows modeling more complex light-attribute interactions.

Another method that works for radiometrically uncalibrated setup is [21] that applies pixel-wise TPS to projector compensation, we combine SL [42] geometric correction with it and name the method **TPS+SL**. Since SL can only recover



Fig. 6: **Projector compensation.** We provide two setups in two rows and compare DeLTra with TPS+SL and CompenNet++. Each image is provided with two zoomed-in patches for detailed comparison.

Table 2: Quantitative comparison of projector compensation. Results are averaged over 10 different setups.

Model	PSNR $\uparrow$	RMSE $\downarrow$	SSIM $\uparrow$	Model	PSNR $\uparrow$	RMSE $\downarrow$	SSIM $\uparrow$
TPS+SL	21.3601	0.1541	0.8695	DeLTra	23.8245	0.1132	0.8885
CompenNet++	22.2046	0.1421	0.8838	Uncompensated	9.3374	0.5979	0.1089

direct light pixels as shown in Fig. 5, for fair comparison, we compare with TPS+SL only on SL masked regions and name it **SL Masked** in Tab. 1. DeLTra outperforms TPS+SL when more than 50 training images are used. However, TPS+SL uses 42 extra SL images to find pixel mappings. Moreover, TPS+SL cannot estimate indirect light as shown in the **Whole Image** columns in Tab. 1.

**Compensation** We compare with TPS+SL and CompenNet++ using the same textured sampling images and we train CompenNet++ for 1’500 iterations. The quantitative results are shown in Tab. 2. Note DeLTra outperforms both TPS+SL and CompenNet++ on PSNR/RMSE by a significant margin. Moreover, as shown in Fig. 6 that DeLTra also produces more visually pleasing compensation results. Our explanations are (1) The novel architecture and domain knowledge let DeLTra better model projector-camera light transport. (2) Explicitly modeling geometry allows DeLTra to deal with more complex scenarios, such as occlusions and partial projector FOV out-of-view. (3) We explicitly deal with saturation errors due to projector’s physical limitation and encourages compensation image smoothness.

**Depth and normal estimation** Besides comparing with the ground truth, we also compare the point cloud reconstructed by SL [42] before it is manually cleaned and interpolated, the error metric is  $\mathbf{d}_{\text{err}} = 1.0858$ . Note this already gives SL [42] great advantages. The qualitative and quantitative results



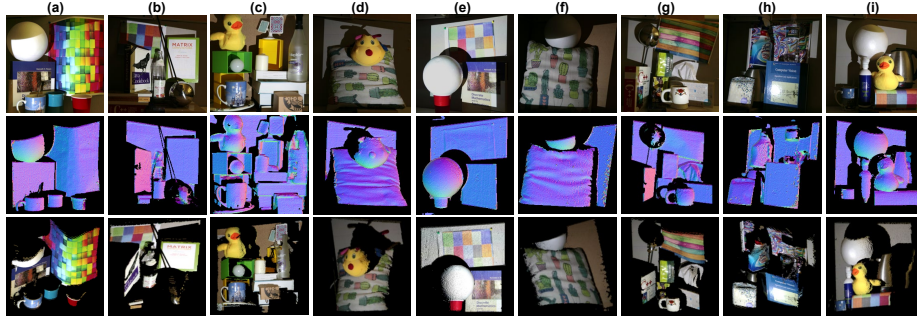


Fig. 7: **Depth and normal reconstruction.** We show nine setups in different columns. The **1st row** is the scene under plain illumination. The **2nd row** is estimated normal. The **3rd row** is reconstructed colored point cloud viewed from a different pose. See [supplementary material](#) for more results.

are shown in [Fig. 7](#) and [Tab. 1](#), respectively. As we can see that the proposed DeLTra shows good depth and normal reconstruction capability, especially when more training images are used.

**Ablation study** To show the effectiveness of the differentiable direct light mask and the domain knowledge, we perform comprehensive ablation studies. For each feature, we create a degraded DeLTra with that feature disabled, *i.e.*, **No rough**, **No mask** and **No const** are w/o rough diffuse and specular shading, w/o direct light mask consistency, and w/o rough shading consistency, respectively. The results in [Tab. 1](#) clearly show that DeLTra outperforms different degraded counterparts, demonstrating that the novel structure, differentiable direct light mask, rough shadings and consistency losses together facilitate the projector-camera light transport problem. See [supplementary material](#) for more results.

## 6 Conclusions and Limitations

In this paper, we propose the first end-to-end trainable method, DeLTra, to estimate radiometrically uncalibrated projector-camera light transport, and apply DeLTra to three tasks: image-based relighting, projector compensation and depth/normal reconstruction. In DeLTra, a novel differentiable direct light mask is proposed to explicitly address occlusions. Its effectiveness is shown by thorough experiments. In addition, it can be easily applied to other learning problems due to its differentiability. Moreover, we incorporate multiple domain knowledge such as direct light mask consistency, rough shading consistency and smoothness constraint, they together bring DeLTra boosted robustness and performance. In our thorough experiments, DeLTra shows clear advantages over previous arts with promising quality and meanwhile being practically convenient.

**Limitations and future work.** DeLTra’s relighting and depth/normal reconstruction are less accurate on indirect light due to our direct light dominance assumption, as shown in [Fig. 5](#) and [Fig. 7](#). Incorporating domain knowledge of light transport matrix and projector-camera radiometric responses may improve the results and it is definitely an interesting direction to explore in future work.

## References

1. Aliaga, D.G., Yeung, Y.H., Law, A., Sajadi, B., Majumder, A.: Fast high-resolution appearance editing using superimposed projections. *ACM Tran. on Graphics* (2012) [1](#), [3](#)
2. Arvo, J., Torrance, K., Smits, B.: A framework for the analysis of error in global illumination algorithms. In: *SIGGRAPH*. pp. 75–84 (1994) [6](#)
3. Ashdown, M., Okabe, T., Sato, I., Sato, Y.: Robust content-dependent photometric projector compensation. In: *CVPRW PROCAMS* (2006) [1](#), [3](#)
4. Bai, J., Chandraker, M., Ng, T.T., Ramamoorthi, R.: A dual theory of inverse and forward light transport. In: *ECCV*. pp. 294–307. Springer (2010) [3](#)
5. Barron, J.T., Malik, J.: Shape, illumination, and reflectance from shading. *T-PAMI* **37**(8), 1670–1687 (2014) [4](#)
6. Bimber, O., Iwai, D., Wetzstein, G., Grundhöfer, A.: The visual computing of projector-camera systems. In: *Computer Graphics Forum*. p. 84 (2008) [1](#), [3](#), [4](#)
7. Blinn, J.F.: Models of light reflection for computer synthesized pictures. In: *SIGGRAPH*. pp. 192–198. No. 2, ACM (1977) [2](#), [6](#)
8. Boroomand, A., Sekkati, H., Lamm, M., Clausi, D.A., Wong, A.: Saliency-guided projection geometric correction using a projector-camera system. In: *ICIP* (2016) [1](#)
9. Chandraker, M., Bai, J., Ng, T.T., Ramamoorthi, R.: On the duality of forward and inverse light transport. *T-PAMI* **33**(10), 2122–2128 (2011) [3](#)
10. Chen, G., Han, K., Shi, B., Matsushita, Y., Wong, K.Y.K.: Self-calibrating deep photometric stereo networks. In: *CVPR*. pp. 8739–8747 (2019) [3](#), [4](#)
11. Chiba, N., Hashimoto, K.: Ultra-fast multi-scale shape estimation of light transport matrix for complex light reflection objects. In: *ICRA*. pp. 1–5. IEEE (2018) [1](#), [3](#), [4](#)
12. Debevec, P., Hawkins, T., Tchou, C., Duiker, H.P., Sarokin, W., Sagar, M.: Acquiring the reflectance field of a human face. In: *SIGGRAPH*. pp. 145–156. ACM Press/Addison-Wesley Publishing Co. (2000) [1](#), [3](#), [6](#)
13. Debevec, P.E., Malik, J.: Recovering high dynamic range radiance maps from photographs. In: *ACM SIGGRAPH 2008 classes*. p. 31. ACM (2008) [2](#), [6](#)
14. Deschaintre, V., Aittala, M., Durand, F., Drettakis, G., Bousseau, A.: Single-image svbrdf capture with a rendering-aware deep network. *ACM Tran. on Graphics* **37**(4), 128 (2018) [4](#)
15. Garg, R., BG, V.K., Carneiro, G., Reid, I.: Unsupervised cnn for single view depth estimation: Geometry to the rescue. In: *ECCV*. pp. 740–756. Springer (2016) [8](#), [9](#)
16. Geng, J.: Structured-light 3D surface imaging: a tutorial. *Advances in Optics and Photonics* (2011) [1](#), [3](#), [4](#)
17. Georgiades, A.S.: Incorporating the torrance and sparrow model of reflectance in uncalibrated photometric stereo. In: *ICCV*. vol. 3, p. 816 (2003) [4](#)
18. Godard, C., Mac Aodha, O., Brostow, G.J.: Unsupervised monocular depth estimation with left-right consistency. In: *CVPR*. pp. 270–279 (2017) [8](#), [9](#)
19. Grossberg, M.D., Nayar, S.K.: Modeling the space of camera response functions. *T-PAMI* **26**(10), 1272–1282 (2004) [2](#), [6](#)
20. Grossberg, M.D., Peri, H., Nayar, S.K., Belhumeur, P.N.: Making one object look like another: controlling appearance using a projector-camera system. In: *CVPR* (2004) [1](#), [3](#)
21. Grundhöfer, A., Iwai, D.: Robust, error-tolerant photometric projector compensation. *IEEE TIP* (2015) [1](#), [3](#), [4](#), [10](#), [12](#)



22. Grundhöfer, A., Iwai, D.: Recent advances in projection mapping algorithms, hardware and applications. In: *Computer Graphics Forum*. Wiley Online Library (2018) [4](#)
23. Guo, K., Lincoln, P., Davidson, P., Busch, J., Yu, X., Whalen, M., Harvey, G., Orts-Escolano, S., Pandey, R., Dourgarian, J., et al.: The relightables: volumetric performance capture of humans with realistic relighting. *ACM Tran. on Graphics* **38**(6), 1–19 (2019) [1](#)
24. Han, S., Sato, I., Okabe, T., Sato, Y.: Fast spectral reflectance recovery using dlp projector. *IJCV* **110**(2), 172–184 (2014) [1](#)
25. Hartley, R., Zisserman, A.: *Multiple view geometry in computer vision*. Cambridge university press (2003) [4](#), [8](#)
26. He, K., Zhang, X., Ren, S., Sun, J.: Deep residual learning for image recognition. In: *CVPR* (2016) [7](#)
27. Hermosilla, P., Maisch, S., Ritschel, T., Ropinski, T.: Deep-learning the latent space of light transport. In: *Computer Graphics Forum*. vol. 38, pp. 207–217. Wiley Online Library (2019) [3](#), [4](#)
28. Huang, B., Ling, H.: Compennet++: End-to-end full projector compensation. In: *ICCV* (2019) [1](#), [4](#), [6](#), [10](#), [11](#), [12](#)
29. Huang, B., Ling, H.: End-to-end projector photometric compensation. In: *CVPR* (2019) [1](#), [4](#), [10](#)
30. Huang, B., Ozdemir, S., Tang, Y., Liao, C., Ling, H.: A single-shot-per-pose camera-projector calibration system for imperfect planar targets. In: *2018 IEEE International Symposium on Mixed and Augmented Reality Adjunct (ISMAR-Adjunct)*. pp. 15–20. IEEE (2018) [7](#), [11](#)
31. Hur, J., Roth, S.: Mirrorflow: Exploiting symmetries in joint optical flow and occlusion estimation. In: *ICCV*. pp. 312–321 (2017) [8](#)
32. Jaderberg, M., Simonyan, K., Zisserman, A., Kavukcuoglu, K.: Spatial transformer networks. In: *NIPS* (2015) [2](#), [9](#)
33. Kajiya, J.T.: The rendering equation. In: *SIGGRAPH*. pp. 143–150. No. 4, ACM (1986) [5](#)
34. Kingma, D.P., Ba, J.: Adam: A method for stochastic optimization. In: *ICLR* (2015) [11](#)
35. Levoy, M., Hanrahan, P.: Light field rendering. In: *SIGGRAPH*. pp. 31–42. ACM (1996) [1](#), [2](#), [3](#)
36. Li, C., Monno, Y., Hidaka, H., Okutomi, M.: Pro-cam ssfm: Projector-camera system for structure and spectral reflectance from motion. In: *ICCV*. pp. 2414–2423 (2019) [3](#), [4](#)
37. Li, T.M., Aittala, M., Durand, F., Lehtinen, J.: Differentiable monte carlo ray tracing through edge sampling. In: *SIGGRAPH Asia*. p. 222. ACM (2018) [3](#), [4](#)
38. Li, X., Dong, Y., Peers, P., Tong, X.: Modeling surface appearance from a single photograph using self-augmented convolutional neural networks. *ACM Tran. on Graphics* **36**(4), 45 (2017) [4](#)
39. Li, Z., Xu, Z., Ramamoorthi, R., Sunkavalli, K., Chandraker, M.: Learning to reconstruct shape and spatially-varying reflectance from a single image. In: *SIGGRAPH Asia*. p. 269. ACM (2018) [4](#)
40. Masselus, V., Peers, P., Dutré, P., Willems, Y.D.: Relighting with 4d incident light fields. *ACM Tran. on Graphics* **22**(3), 613–620 (2003) [1](#), [3](#)
41. Meister, S., Hur, J., Roth, S.: Unflow: Unsupervised learning of optical flow with a bidirectional census loss. In: *AAAI* (2018) [8](#)
42. Moreno, D., Taubin, G.: Simple, accurate, and robust projector-camera calibration. In: *3DIMPVT* (2012) [1](#), [3](#), [4](#), [11](#), [12](#), [13](#)

43. Nair, V., Hinton, G.E.: Rectified linear units improve restricted boltzmann machines. In: ICML (2010) [9](#)
44. Nalbach, O., Arabadzhyska, E., Mehta, D., Seidel, H.P., Ritschel, T.: Deep shading: convolutional neural networks for screen space shading. In: Computer Graphics Forum. vol. 36, pp. 65–78. Wiley Online Library (2017) [3](#), [4](#)
45. Narita, G., Watanabe, Y., Ishikawa, M.: Dynamic projection mapping onto deforming non-rigid surface using deformable dot cluster marker. IEEE TVCG (2017) [1](#), [3](#)
46. Nayar, S.K., Krishnan, G., Grossberg, M.D., Raskar, R.: Fast separation of direct and global components of a scene using high frequency illumination. In: ACM Tran. on Graphics. vol. 25, pp. 935–944. ACM (2006) [1](#), [4](#)
47. Nayar, S.K., Peri, H., Grossberg, M.D., Belhumeur, P.N.: A projection system with radiometric compensation for screen imperfections. In: ICCVW PROCAMS. vol. 3 (2003) [1](#), [3](#)
48. Ng, R., Ramamoorthi, R., Hanrahan, P.: All-frequency shadows using non-linear wavelet lighting approximation. In: ACM Tran. on Graphics. vol. 22, pp. 376–381. ACM (2003) [3](#)
49. Ng, T.T., Pahwa, R.S., Bai, J., Quek, T.Q., Tan, K.H.: Radiometric compensation using stratified inverses. In: ICCV. pp. 1889–1894. IEEE (2009) [3](#)
50. Ng, T.T., Pahwa, R.S., Bai, J., Tan, K.H., Ramamoorthi, R.: From the rendering equation to stratified light transport inversion. International Journal of Computer Vision **96**(2), 235–251 (2012) [3](#), [6](#)
51. O’Toole, M., Kutulakos, K.N.: Optical computing for fast light transport analysis. ACM Tran. on Graphics **29**(6), 164 (2010) [1](#), [2](#)
52. O’Toole, M., Mather, J., Kutulakos, K.N.: 3d shape and indirect appearance by structured light transport. In: T-PAMI. pp. 1298–1312 (2016) [1](#), [3](#), [4](#), [6](#)
53. Oya, S., Okabe, T.: Image-based relighting with 5-d incident light fields. In: ICCV. pp. 3031–3038 (2017) [1](#), [3](#)
54. Paszke, A., Gross, S., Chintala, S., Chanan, G., Yang, E., DeVito, Z., Lin, Z., Desmaison, A., Antiga, L., Lerer, A.: Automatic differentiation in pytorch. In: NIPS-W (2017) [11](#)
55. Peers, P., Mahajan, D.K., Lamond, B., Ghosh, A., Matusik, W., Ramamoorthi, R., Debevec, P.: Compressive light transport sensing. ACM Tran. on Graphics **28**(1), 3 (2009) [1](#), [3](#)
56. Phong, B.T.: Illumination for computer generated pictures. Communications of the ACM **18**(6), 311–317 (1975) [2](#), [6](#)
57. Qi, X., Liao, R., Liu, Z., Urtasun, R., Jia, J.: Geonet: Geometric neural network for joint depth and surface normal estimation. In: CVPR. pp. 283–291 (2018) [4](#)
58. Raskar, R., Beardsley, P.: A self-correcting projector. In: CVPR (2001) [1](#), [3](#)
59. Raskar, R., Van Baar, J., Beardsley, P., Willwacher, T., Rao, S., Forlines, C.: il-amps: geometrically aware and self-configuring projectors. ACM Tran. on Graphics (2003) [1](#), [3](#)
60. Raskar, R., Welch, G., Low, K.L., Bandyopadhyay, D.: Shader lamps: Animating real objects with image-based illumination. In: Rendering Techniques. Springer (2001) [1](#)
61. Ren, P., Dong, Y., Lin, S., Tong, X., Guo, B.: Image based relighting using neural networks. ACM Tran. on Graphics **34**(4), 111 (2015) [1](#), [3](#)
62. Riba, E., Mishkin, D., Ponsa, D., Rublee, E., Bradski, G.: Kornia: an open source differentiable computer vision library for pytorch. In: WACV (2019) [11](#)
63. Ronneberger, O., Fischer, P., Brox, T.: U-net: Convolutional networks for biomedical image segmentation. In: MICCAI. Springer (2015) [6](#)

64. Santo, H., Samejima, M., Sugano, Y., Shi, B., Matsushita, Y.: Deep photometric stereo network. In: ICCV. pp. 501–509 (2017) [3](#), [4](#)
65. Seitz, S.M., Matsushita, Y., Kutulakos, K.N.: A theory of inverse light transport. In: ICCV. vol. 2, pp. 1440–1447. IEEE (2005) [3](#), [6](#)
66. Sen, P., Chen, B., Garg, G., Marschner, S.R., Horowitz, M., Levoy, M., Lensch, H.: Dual photography. In: ACM Tran. on Graphics. vol. 24, pp. 745–755. ACM (2005) [1](#), [3](#), [6](#)
67. Shafer, S.A.: Using color to separate reflection components. Color Research & Application **10**(4), 210–218 (1985) [2](#), [6](#)
68. Shi, B., Tan, P., Matsushita, Y., Ikeuchi, K.: Bi-polynomial modeling of low-frequency reflectances. T-PAMI **36**(6), 1078–1091 (2013) [4](#)
69. Shi, B., Wu, Z., Mo, Z., Duan, D., Yeung, S.K., Tan, P.: A benchmark dataset and evaluation for non-lambertian and uncalibrated photometric stereo. In: T-PAMI. pp. 271–284 (2019) [3](#), [4](#)
70. Siegl, C., Colaianni, M., Thies, L., Thies, J., Zollhöfer, M., Izadi, S., Stamminger, M., Bauer, F.: Real-time pixel luminance optimization for dynamic multi-projection mapping. ACM Tran. on Graphics (2015) [1](#), [3](#)
71. Sueishi, T., Oku, H., Ishikawa, M.: Robust high-speed tracking against illumination changes for dynamic projection mapping. In: IEEE VR. pp. 97–104. IEEE (2015) [1](#)
72. Tani, T., Maehara, T.: Neural inverse rendering for general reflectance photometric stereo. In: ICML. pp. 4864–4873 (2018) [3](#), [4](#)
73. Tardif, J.P., Roy, S., Trudeau, M.: Multi-projectors for arbitrary surfaces without explicit calibration nor reconstruction. In: 3DIM (2003) [1](#)
74. Vo, M., Narasimhan, S.G., Sheikh, Y.: Texture illumination separation for single-shot structured light reconstruction. T-PAMI **38**(2), 390–404 (2015) [1](#), [3](#), [4](#)
75. Wang, J., Dong, Y., Tong, X., Lin, Z., Guo, B.: Kernel nystrom method for light transport. ACM Tran. on Graphics **28**(3), 29 (2009) [1](#), [2](#), [3](#)
76. Wang, Y., Yang, Y., Yang, Z., Zhao, L., Wang, P., Xu, W.: Occlusion aware unsupervised learning of optical flow. In: CVPR. pp. 4884–4893 (2018) [8](#)
77. Wenger, A., Gardner, A., Tchou, C., Unger, J., Hawkins, T., Debevec, P.: Performance relighting and reflectance transformation with time-multiplexed illumination. In: ACM Tran. on Graphics. vol. 24, pp. 756–764. ACM (2005) [3](#)
78. Woodham, R.J.: Photometric method for determining surface orientation from multiple images. Optical engineering **19**(1), 191139 (1980) [3](#), [4](#)
79. Yoshida, T., Horii, C., Sato, K.: A virtual color reconstruction system for real heritage with light projection. In: Proceedings of International Conference on Virtual Systems and Multimedia. vol. 3 (2003) [1](#), [3](#)
80. Yu, Y., Smith, W.A.: Inverserendernet: Learning single image inverse rendering. In: CVPR. pp. 3155–3164 (2019) [4](#)
81. Zhao, H., Gallo, O., Frosio, I., Kautz, J.: Loss functions for image restoration with neural networks. IEEE TCI (2017) [10](#)
82. Zhou, T., Brown, M., Snively, N., Lowe, D.G.: Unsupervised learning of depth and ego-motion from video. In: CVPR. pp. 1851–1858 (2017) [9](#)
83. Zongker, D.E., Werner, D.M., Curless, B., Salesin, D.: Environment matting and compositing. In: SIGGRAPH. vol. 99, pp. 205–214 (1999) [1](#), [3](#), [6](#)